Ablation of IL-33 Suppresses *Th2* Responses but Is Accompanied by Sustained Mucus Obstruction in the *Scnn1b* Transgenic Mouse Model

Brandon W. Lewis,*,[1] Thao Vo,*,[1] Ishita Choudhary,*,[1] Allison Kidder,* Chandra Bathula,* Camille Ehre,[†] Nobuko Wakamatsu,[‡] Sonika Patial,* and Yogesh Saini*

Cystic fibrosis is characterized by dehydration of the airway surface liquid layer with persistent mucus obstruction. *Th2* immune responses are often manifested as increased mucous cell density (mucous cell metaplasia) associated with mucus obstruction. IL-33 is a known inducer of *Th2* immune responses, but its roles in mucus obstruction and related phenotypes in a cystic fibrosis–like lung disease model (i.e., *Scnn1b*-Tg–positive [Tg+]) mouse, remain unclear. Accordingly, IL-33 knockout (IL-33^{KO}) Tg+ mice were examined and compared with IL-33 heterozygous (IL-33^{HET}) Tg+ mice. As compared with IL-33^{HET}/Tg+ mice, IL-33^{KO}/Tg+ mice had complete absence of bronchoalveolar lavage fluid eosinophilia, accompanied with significant reduction in bronchoalveolar lavage fluid concentration of IL-5, a cytokine associated with eosinophil differentiation and recruitment, and IL-4, a major *Th2* cytokine. As compared with IL-33^{HET}/Tg+ mice, IL-33^{KO}/Tg+ mice had significantly reduced levels of *Th2*-associated gene signatures (*Slc26a4*, *Clca1*, *Retnla*, and *Chi3l4*), along with complete loss of intracellular mucopolysaccharide staining in the airway epithelium. As compared with IL-33^{HET}/Tg+ mice, although the IL-33^{KO}/Tg+ mice had significantly reduced levels of MUC5AC protein expression, they showed no reduction in the degree of mucus obstruction, MUC5B protein expression, bacterial burden, and neonatal mortality. Interestingly, the histological features, including subepithelial airway inflammation and alveolar space enlargement, were somewhat exaggerated in IL-33^{KO}/Tg+ mice compared with IL-33^{HET}/Tg+ mice. Taken together, our data indicate that although IL-33 modulates *Th2* inflammatory responses and MUC5AC protein production, mucus obstruction is not dependent on IL-33. ***The Journal of Immunology*****, 2020, 204: 1650–1660.**

Airway mucosal surfaces are lined by a thin layer of liquid (i.e., the airway surface liquid [ASL]) consisting of water, ions, proteins, and macromolecules, including mucin glycoproteins (1). Optimal solid contents of the ASL layer are essential for the proper functioning of the mucociliary apparatus that propels the mucus layer with entrapped airborne particles toward the epiglottis (1). The dysfunction of the cystic fibrosis (CF) transmembrane conductance regulator in CF airways induces ionic imbalance that results in dehydration of the ASL layer and an associated increase in solid contents in the ASL layer and consistent mucus obstruction (2, 3). In addition to ASL dehydration, mucoinflammatory responses (i.e., excessive mucin production accompanied with increased inflammatory cell density and cellular debris) may also result in increased ASL solid contents and, ultimately, contribute to the mucus obstruction. Therefore, it is unclear whether the CF-like muco-obstructive phenotype is due to ASL dehydration alone or mucoinflammatory responses alone or a combination of both. Whereas investigating these scenarios is challenging in human CF patients, the *Scnn1b* transgenic–positive (Tg+) mouse is an ideal model for experimental testing, as it manifests CF-like lung disease.

The Tg+ mouse model overexpresses the sodium channel non–voltage gated 1 β subunit (*Scnn1b*) in the airway epithelial cells that induces epithelial water hyperabsorption, resulting in a phenocopy of CF-like ASL dehydration (4, 5). The Tg+ mice exhibit robust *Th2* mucoinflammatory airway pathology with marked mucous cell metaplasia (MCM) and increased molecular markers of *Th2* inflammation (5–7). These responses are associated with mucus obstruction that provides a fertile nidus for bacterial colonization (5). IL-33 has been shown to be a potent stimulator of

*Department of Comparative Biomedical Sciences, Louisiana State University, Baton Rouge, LA 70803; [†]Marsico Lung Institute, School of Medicine, University of North Carolina at Chapel Hill, Chapel Hill, NC 27599; and [‡]Department of Pathobiological Sciences, Louisiana State University, Baton Rouge, LA 70803

[1]B.W.L., T.V., and I.C. contributed equally to this work.

ORCIDs: 0000-0002-6962-3316 (B.W.L.); 0000-0001-8242-3928 (I.C.); 0000-0001-9110-4347 (C.B.); 0000-0002-4342-8934 (S.P.); 0000-0002-8324-2122 (Y.S.).

Received for publication February 25, 2019. Accepted for publication January 14, 2020.

This work was supported by a Flight Attendant Medical Research Institute grant (to Y.S.), National Institute of General Medical Sciences Grant 5P30GM110760 (Pilot Project Funding), National Institute of General Medical Sciences Grant P20GM130555 (to Y.S.), and National Institute of Environmental Health Sciences Grant R01ES030125 (to Y.S.).

Y.S. conceived and designed the study; B.W.L., T.V., I.C., A.K., and Y.S. maintained the animal colony, conducted animal necropsies, and performed bronchoalveolar lavage fluid cellularity assays; Y.S., B.W.L., T.V., C.B., and S.P. performed cytokine, ELISA, gene expression assays, and histopathological experiments; B.W.L. and Y.S. performed microbiological analyses; N.W. and S.P. performed histopathological analyses; B.W.L., C.E., and Y.S. performed immunohistochemical staining; Y.S., S.P., and B.W.L. wrote and reviewed the manuscript for intellectual contents.

Address correspondence and reprint requests to Dr. Yogesh Saini, Department of Comparative Biomedical Sciences, School of Veterinary Medicine, 1909 Skip Bertman Drive, Louisiana State University, Baton Rouge, LA 70803. E-mail address: ysaini@lsu.edu

The online version of this article contains supplemental material.

Abbreviations used in this article: AB-PAS, Alcian blue–periodic acid Schiff; ACD, Advanced Cell Diagnostics; ASL, airway surface liquid; BALF, bronchoalveolar lavage fluid; CF, cystic fibrosis; IL-33^{KO}, IL-33 knockout; IL-33^{HET}/Tg+, IL-33 heterozygous Tg+; KC, keratinocyte chemoattractant; MCM, mucous cell metaplasia; MLI, mean linear intercept; PND, postnatal day; *Scnn1b*, sodium channel non–voltage gated 1 β subunit; Tg+, *Scnn1b*-Tg–positive; SHS, secondhand smoke; Tg, transgenic; WT, wild-type.

Th2 inflammation (8). Our recent report identified an intriguing association between reduced IL-33 expression and diminished *Th2* mucoinflammatory responses (e.g., MCM, mucus obstruction, and molecular markers of *Th2* inflammation) (9). However, it remains to be mechanistically tested whether the germline deletion of IL-33 prevents *Th2* responses and mucus obstruction in Tg+ mice.

In this study, we hypothesized that IL-33 is essential for *Th2* inflammatory responses that contribute to the mucus obstruction in the airways of Tg+ mice. To test this hypothesis, IL-33 knockout Tg+ (IL-33^{KO}/Tg+) mice were generated and compared with IL-33 heterozygous Tg+ (IL-33^{HET}/Tg+) mice for various pathological manifestations of CF-like muco-obstructive lung disease. Specifically, the effects of IL-33 deletion on 1) inflammatory cell recruitment, 2) levels of inflammatory mediators, 3) clearance of spontaneous bacterial infection, 4) neonatal mortality, 5) presence of mucous secretory cells, and 6) mucus obstruction were determined. Importantly, we also determined the effects of IL-33 deletion on the mRNA and protein expression levels of two major gel-forming mucins, MUC5B and MUC5AC. The results from this study delineate the contribution of IL-33 to the mucoinflammatory responses in CF-like lung disease with dehydrated ASL layer.

Materials and Methods

Generation of Tg mice and animal husbandry

Tg+ mice (*Tg(Scgb1a1-Scnn1b)6608Bouc/J*) were procured from The Jackson Laboratory (Bar Harbor, ME), and IL-33 knockout (IL-33^{KO}) mice were generously provided by Dr. Susumu Nakae (University of Tokyo, Tokyo, Japan) (10). Both of these mice strains were on C57BL/6 background. These two strains were crossbred to generate IL-33 knockout Tg+ (IL-33^{KO}/Tg+) and IL-33 heterozygous Tg+ (IL-33^{HET}/Tg+) mice, and their Tg− (wild-type [WT]) counterparts. Various genetic combinations (e.g., IL-33^{HET}/WT, IL-33^{KO}/WT, IL-33^{HET}/Tg+, and IL-33^{KO}/Tg+) were generated by reciprocal crosses between IL-33^{HET}/Tg+ and IL-33^{KO}/WT mice, and in parallel, by reciprocal crosses between IL-33^{HET}/WT and IL-33^{KO}/Tg+ mice. Genotyping of experimental mice was performed by PCR as previously described for the presence of Tg+ and *Il33* (Supplemental Fig. 1) (5, 10). Mice were maintained in individually ventilated, hot-washed cages at the Division of Laboratory Animal Medicine (Louisiana State University, Baton Rouge, LA) on a 12 h dark/light cycle. Mice were fed regular diet and water ad libitum. All animal use procedures were approved by the Institutional Animal Care and Use Committee of Louisiana State University.

Bronchoalveolar lavage fluid analyses

Aseptically harvested bronchoalveolar lavage fluid (BALF) was serially diluted onto Columbia Blood Agar plates (Hardy Diagnostics, Santa Maria, CA) as previously described (9, 11, 12). The Columbia Blood Agar plates were incubated in an anaerobic candle jar for 48 h at 37°C. Bacterial burden was determined by enumerating CFUs. Remaining BALF was centrifuged at 300 × *g* for 5 min. The supernatant was removed and stored at −80°C for cytokine analyses. The cellular pellet was resuspended in 500 μl of PBS. Total cell counts were determined using a hemocytometer (Bright-Line, Horsham, PA). Cytospins (Cytospin 3; Thermo Scientific Shandon, Pittsburgh, PA) were prepared with a 200 μl cell suspension and differentially stained (Modified Giemsa kit; Newcomer Supply, Middleton, WI).

Analyses of BALF for cytokines

Cell-free BALF was assayed for various cytokines (Table I) using a Luminex xMAP-based assay (MCYTOMAG-70K) according to the manufacturer's instructions (EMD Millipore, Billerica, MA). To estimate IL-33 concentration, cell-free BALF supernatant or lung homogenate supernatant was assayed with a Mouse/Rat IL-33 ELISA Kit (M3300) according to the manufacturer's instructions (R&D Systems, Minneapolis, MN). In the case of tissue IL-33 estimation assay, the right middle lobe was homogenized in 500 μl of radioimmunoprecipitation assay buffer containing protease inhibitors.

Histopathological analyses

Left lung lobes were formalin-fixed, paraffin embedded, sectioned, and stained for histopathological analyses. Histopathological parameters were compared by blinded board-certified pathologists (S. Patial and N. Wakamatsu) using a previously described semiquantitative grading strategy (13). Briefly, histological sections stained with H&E were used to evaluate histopathological changes. To evaluate mucus obstruction and MCM, histological slides were stained with Alcian blue–periodic acid Schiff (AB-PAS). Mucous cell density (number of mucous cells per millimeter of basement membrane) was used as a quantitative parameter to evaluate MCM, using ×40 objective of Nikon Eclipse Ci light microscope with camera attachment (Nikon Digital Sight DSFi2). Airway epithelial cells (at least 50 cells) and mucous cells, distinguished by presence of AB-PAS staining, were counted.

Gene expression analyses

Total RNA was extracted and analyzed for quantity and purity as described previously (9). cDNA generation and RT-PCR were done to assess the gene expression signals of selected genes *Slc26a4*, *Clca1*, *Retnla*, *Chi3l4*, *Muc5b*, and *Muc5ac*, as described previously (9).

Mucins agarose gel electrophoresis and Western blotting

BALF mucin electrophoresis and Western blotting were performed using a slightly modified protocol, as described previously (14). Briefly, BALF mucins were denatured with urea (6 M). Equal volumes (50 μl per well) of BALF samples were electrophoresed on 1% agarose gel (at 80 V for 90 min) and vacuum blotted onto nitrocellulose membranes with 4× sodium saline citrate buffer for 2 h at −50 mBar pressure. After transfer, the nitrocellulose membrane was blocked with blocking buffer (LI-COR Biosciences, Lincoln, NE) for 1 h at room temperature, followed by primary Ab incubation (overnight at 4°C) with rabbit polyclonal Abs against MUC5B (UNC223; University of North Carolina, Chapel Hill, NC) and mouse mAbs against MUC5AC (AB3649; Abcam, Cambridge, MA). After washing, the membrane was probed with IRDye 680RD Goat anti-Rabbit and IRDye 800CW Goat anti-Mouse IgG (LI-COR Biosciences) secondary Abs, each diluted to 1:5000 in blocking buffer. After 1 h of incubation at room temperature, the membrane was analyzed by the Odyssey CLx Infrared Imaging System (LI-COR Biosciences). The band intensity was measured using Image J software (National Institutes of Health).

RNAScope (RNA in situ hybridization)

To assess the distribution and relative abundance of *Muc5b* and *Muc5ac* transcripts, in situ hybridization was performed on paraffin-embedded airway sections using Advanced Cell Diagnostics (ACD) proprietary RNAScope Technology (ACD, Newark, CA). Predesigned transcript-specific probes were used to hybridize *Muc5b* and *Muc5ac* transcripts in the airway sections, and an RNAScope 2.5 HD Duplex Assay Kit (ACD) was used to amplify the transcript signals. *Muc5b* and *Muc5ac* amplification signals were detected as green and red staining, respectively.

Mean linear intercept measurements

Briefly, two different lung sections per mouse were imaged at 10× magnification using a Nikon scope (Nikon) with camera attachment (Nikon Digital Sight DSFi2). Images were loaded onto Image J software and converted to binary. Horizontal grid lines were superimposed on the lung section image. Using line drawing software, lines were drawn along gridlines and measured. Intercepts were considered as points of contact between the drawn line and alveolar septi. Mean linear intercepts (MLI) were determined by dividing the sum of the length of all drawn lines (micrometers) by the sum of the total intercepts between alveolar septi and drawn lines (15).

Statistical analyses

One-way ANOVA followed by Tukey post hoc test for multiple comparisons was used to determine significant differences among groups. Measurements from two groups were compared using Student *t* test assuming unequal variance. All data were expressed as mean ± SEM. A p value < 0.05 was considered statistically significant. Statistical analyses were performed using GraphPad Prism 7.0 (GraphPad Software, La Jolla, CA).

Results

IL-33 contents are elevated in the BALF and lung tissue of Tg+ mice

To identify the age at which IL-33 is released into the airspaces of Tg+ mice, IL-33 contents were estimated in BALF from WT and Tg+ neonates (postnatal day [PND] 7) and juveniles (PND 21). IL-33 protein was undetectable in BALF from WT as well as Tg+ neonates (Fig. 1A, left panel). Although IL-33 protein was undetectable in BALF from WT juveniles, the Tg+ juveniles had significantly elevated levels of IL-33 (Fig. 1A, right panel).

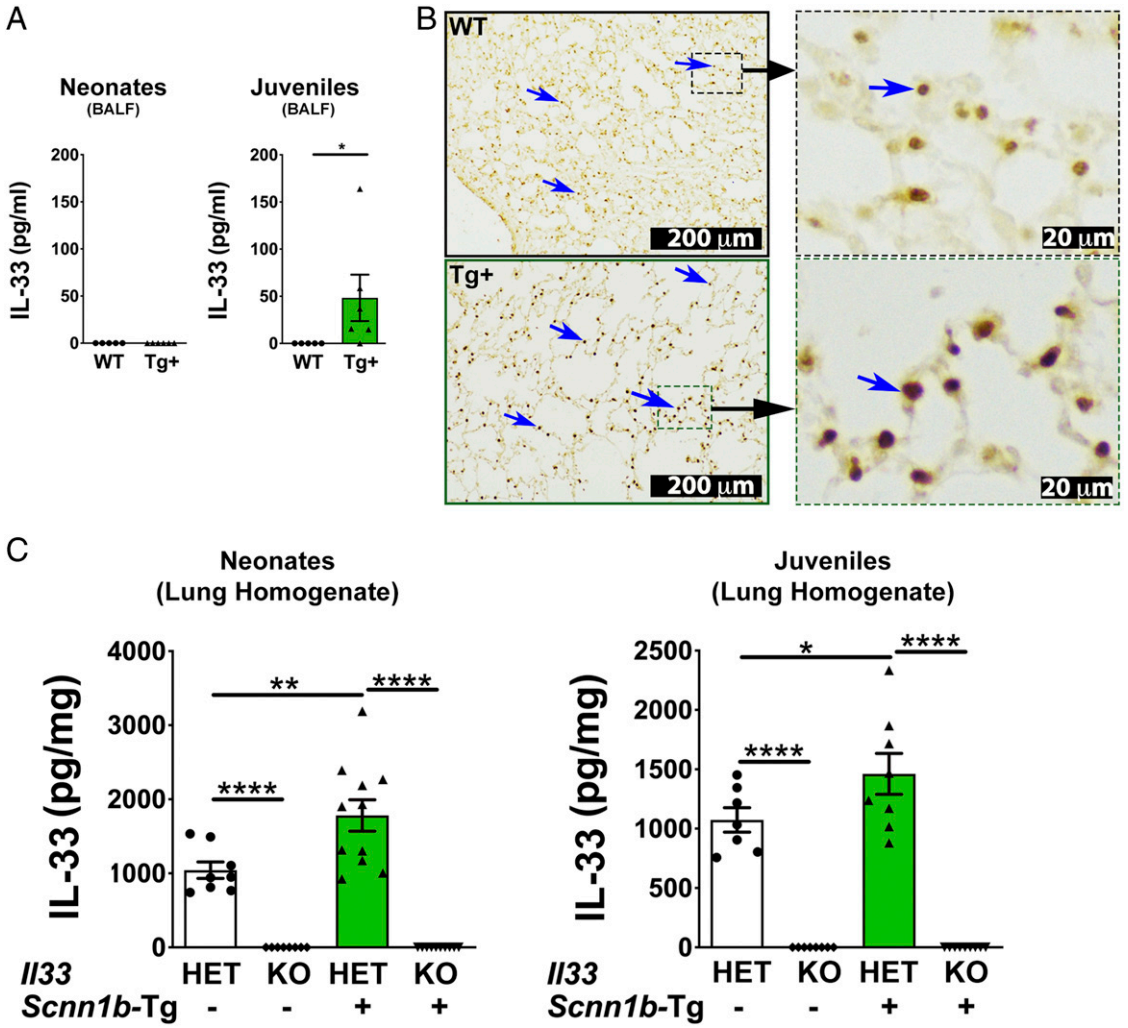

FIGURE 1. IL-33 protein contents are elevated in the Tg+ lungs. IL-33 concentration in cell-free BALF from WT (white bar) and Tg+ (green bar) neonates (**A**, left) and juveniles (A, right) (n = 5–6 per group). For IL-33 estimation in BALF, because equal volumes of BALF samples were used, the estimated IL-33 values in picograms per milliliter were used directly. Error bars represent SEM. *$p < 0.05$ using Student t test. Representative photomicrographs from lung sections showing immunolocalization of IL-33 protein (blue arrows) in WT juveniles (**B**) (top left and top right, higher magnification) and Tg+ juveniles (B) (bottom left and bottom right, higher magnification). IL-33 concentration in picograms per milligram in lung homogenates from WT (white bar) and Tg+ (green bar) neonates (**C**, left) and juveniles (C, right) (n = 8–11 per group). The estimated IL-33 values were normalized to the total lung homogenate protein content. Error bars represent SEM. *$p < 0.05$, **$p < 0.01$, ****$p < 0.0001$ using ANOVA followed by Tukey multiple comparison post hoc test.

To identify the cellular source of IL-33 in Tg+ lungs, we performed immuno-histochemical staining for IL-33 in lung sections from WT and Tg+ juveniles. Although IL-33 was found to be localized in the alveolar epithelial cells of both WT and Tg+ juveniles, the IL-33 staining was remarkably intense in alveolar epithelial cells from Tg+ juveniles (Fig. 1B). Further, the level of IL-33 protein in the lung homogenates from WT and Tg+ mice on IL-33^{HET} or IL-33^{KO} background were assessed (Fig. 1C). As compared with IL-33^{HET}/WT neonates and IL-33^{HET}/WT juveniles, the total IL-33 contents were significantly higher in both IL-33^{HET}/Tg+ neonates (Fig. 1C, left panel) and IL-33^{HET}/Tg+ juveniles (Fig. 1C, right panel). As expected, IL-33 was undetected in the lung homogenates from both IL-33^{KO}/WT and IL-33^{KO}/Tg+ neonates (Fig. 1C, left panel) and juveniles (Fig. 1C, right panel).

IL-33 deletion modulates immune cell recruitment in juvenile Tg+ airways

To determine the effect of IL-33 deletion on immune cell recruitment into the Tg+ airspaces of juveniles, BALF samples were analyzed for alterations in the inflammatory cell counts and soluble inflammatory mediators. The IL-33^{KO}/WT and IL-33^{HET}/WT mice had a comparable number of total immune cells in their BALF (Fig. 2A). The proportion of individual immune cells, including macrophages, neutrophils, eosinophils, and lymphocytes, were also comparable among IL-33^{KO}/WT and IL-33^{HET}/WT mice (Fig. 2B, 2C). The IL-33^{HET}/Tg+ mice had a significant increase in the number of total BALF cells as a result of an increase in three cell types (e.g., neutrophils, eosinophils, and lymphocytes) (Fig. 2B, 2C). The total cell, macrophage, neutrophil, and lymphocyte counts in IL-33^{KO}/Tg+ BALF were comparable to BALF cell counts obtained from IL-33^{HET}/Tg+ littermates (Fig. 2B, 2C). Nonetheless, the eosinophilic counts were significantly lower in the IL-33^{KO}/Tg+ BALF as compared with IL-33^{HET}/Tg+ BALF (Fig. 2B, 2C).

To determine the effect of IL-33 deletion on chemokine levels in Tg+ airspaces, BALF was assayed for the presence of cell-specific chemokines. Neutrophil chemoattractants, including keratinocyte chemoattractant (KC), MIP2, G-CSF, MIP1α, and MCP-1, were below detection levels in IL-33^{HET}/WT and IL-33^{KO}/WT mice (Fig. 2D–F, Table I). All of these cytokines were significantly elevated but comparable to one another in BALF from IL-33^{HET}/Tg+ and

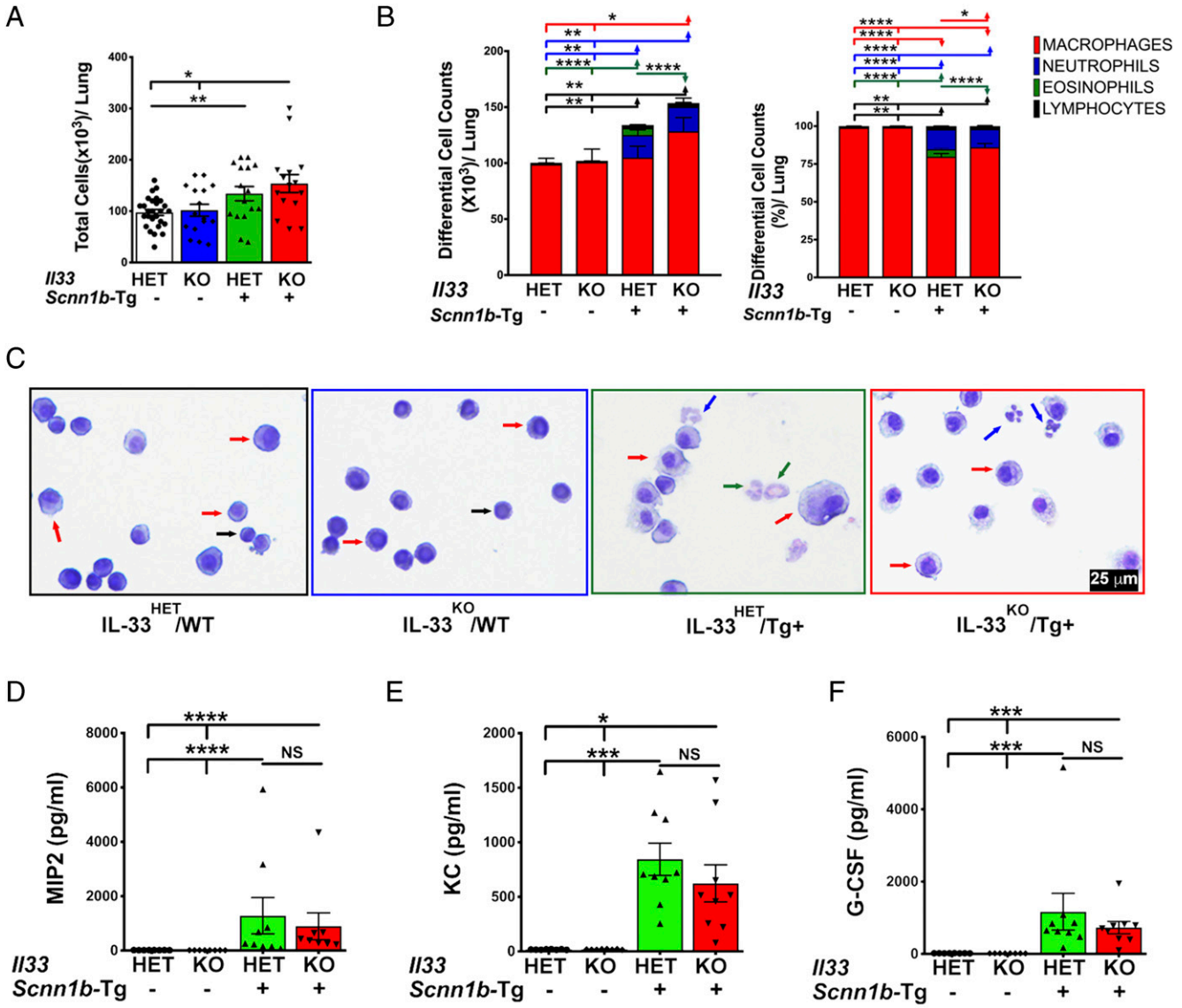

FIGURE 2. IL-33 deficiency alters immune cell recruitment. (**A**) Total cell counts in BALF from IL-33^{HET}/WT (white bar), IL-33^{KO}/WT (blue bar), IL-33^{HET}/Tg+ (green bar), and IL-33^{KO}/Tg+ juveniles (red bar) (n = 15–26 per group). (**B**) Differential cell counts (left) and relative percentages (right) are shown as stacked bar graphs (macrophages [red], neutrophils [blue], eosinophils [green], and lymphocytes [black]). Error bars represent SEM. Significant differences in numbers or proportions of different cell types are indicated by horizontal lines of cell-specific colors (i.e., macrophages [red line], neutrophils [blue line], eosinophils [green line], and lymphocytes [black line]). (**C**) Representative photomicrographs of BALF cytospins from IL-33^{HET}/WT, IL-33^{KO}/WT, IL-33^{HET}/Tg+, and IL-33^{KO}/Tg+ juveniles. Macrophages (red arrow), neutrophils (blue arrow), eosinophils (green arrow), and lymphocytes (black arrow) are shown. BALF cytokine levels (picograms per milliliter) of MIP2 (**D**), KC (**E**), and G-CSF (**F**), in cell-free BALF from IL-33^{HET}/WT (white bar), IL-33^{KO}/WT (blue bar), IL-33^{HET}/Tg+ (green bar), IL-33^{KO}/Tg+ juveniles (red bar). Error bars represent SEM. *$p < 0.05$, **$p < 0.01$, ***$p < 0.001$, ****$p < 0.0001$ using ANOVA followed by Tukey multiple comparison post hoc test. MIP2, macrophage inflammatory protein-2.

IL-33^{KO}/Tg+ mice (Fig. 2D–F, Table I). Eosinophil chemoattractants, IL-5 (Fig. 3A) and RANTES (Table I) were below detection levels in IL-33^{HET}/WT and IL-33^{KO}/WT mice. Both of these mediators were significantly elevated in BALF from IL-33^{HET}/Tg+ mice. However, IL-5 and RANTES were significantly reduced to basal levels in IL-33^{KO}/Tg+ mice (Fig. 3A, Table I).

Deletion of IL-33 results in diminished Th2 inflammation markers in juvenile Tg+ airways

The Tg+ mice predominantly exhibit *Th2* inflammation characterized by elevated levels of eosinophils in BALF, elevated levels of soluble mediators (e.g., IL-4 and IL-5), and elevated levels of *Th2* gene signatures *Slc26a4* (pendrin), *Clca1* (Gob5), *Retnla* (Fizz1), and *Chi3l4* (YM2) (9, 16). In agreement, as presented in the previous section, IL-33^{HET}/Tg+ mice had significant BALF eosinophilia (Fig. 2B, 2C) and a concomitant increase in BALF IL-5 levels (Fig. 3A). Both of these features were completely abolished in IL-33^{KO}/Tg+ juveniles (Figs. 2B, 2C, 3A). Although levels of IL-4 were at baseline in IL-33^{HET}/WT and IL-33^{KO}/WT juveniles, the IL-33^{HET}/Tg+ juveniles had significantly elevated BALF IL-4 levels (Fig. 3B). The BALF from IL-33^{KO}/Tg+ juveniles had significant reduction in IL-4 contents to baseline levels (Fig. 3B).

Th2 inflammation-associated gene signatures were assessed in the total lung RNA preparations. In the absence of *Scnn1b* transgene, the IL-33^{HET} as well as IL-33^{KO} juveniles had baseline levels of expression of four *Th2* inflammation-associated genes [e.g., *Slc26a4* (Fig. 3C), *Clca1* (Fig. 3D), *Retnla* (Fig. 3E), and *Chi3l4* (Fig. 3F)]. Although the levels of all four genes were significantly elevated in IL-33^{HET}/Tg+ lungs, their expression levels were significantly reduced to the baseline level in IL-33^{KO}/Tg+ mice (Fig. 3C–F).

Table I. BALF cytokine levels (picograms per milliliter)

Cytokine	IL-33^{HET}/WT	IL-33^{KO}/WT	IL-33^{HET}/Tg+	IL-33^{KO}/Tg+	LOD
IL-4	10.4 ± 0.18 #	10.5 ± 0.46 π	22.17 ± 4.96 # π	**11.56 ± 0.50**	3.2
IL-5	13.88 ± 0.2#	14.1 ± 0.4 π	42.4 ± 16.0 # π	**14.4 ± 0.3**	3.2
RANTES	26.3 ± 0.5#	24.9 ± 0.7 π	30.1 ± 1.1# π	**26.6 ± 0.8**	3.2
MIP1α	9.25 ± 0.3 # Φ	10.1 ± 0.3 π θ	46.9 ± 8.9 # π	**26.7 ± 2.7 Φ θ**	3.2
IP10	34.6 ± 1.9 # Φ	38.1 ± 2.1 π θ	86.4 ± 15.2 # π	**52.5 ± 5.4 Φ θ**	3.2
MIP1β	31.0 ± 0.9 # Φ	31.2 ± 0.8 π θ	85.0 ± 13.6 # π	**64.6 ± 6.5 Φ θ**	3.2
IL-12 (P70)	26.6 ± 1.0 #	23.3 ± 0.9 π	25.4 ± 1.0 # π	**23.3 ± 0.9**	3.2
KC	16.6 ± 0.8 # Φ	18.3 ± 0.9 π θ	844.7 ± 148.0 # π	623.6 ± 170.1 Φ θ	3.2
IL-6	11.8 ± 0.4 #	12.1 ± 0.5 π θ	53.8 ± 32.6 # π	29.1 ± 8.7 θ	3.2
TNF-α	15.3 ± 0.4 # Φ	15.3 ± 0.3 π θ	28.1 ± 2.4 # π	23.6 ± 1.4 Φ θ	3.2
MIP2	14.6 ± 0.4 # Φ	14.8 ± 0.2 π θ	1282.0 ± 665.8 # π	893.3 ± 495.3 Φ θ	3.2
G-CSF	16.9 ± 0.5 # Φ	14.6 ± 0.5 π θ	1166.0 ± 507.6 # π	727.1 ± 171.1 Φ θ	3.2
IL-17	16.4 ± 0.3 # Φ	15.3 ± 0.5 π θ	22.4 ± 2.8 # π	18.0 ± 0.6 Φ θ	3.2
IL-10	16.4 ± 0.8 #	15.5 ± 0.5	15.1 ± 0.5	14.0 ± 0.6 #	3.2
MCP1	10.2 ± 0.4 #	10.2 ± 0.3 π	11.61 ± 0.5 # π	11.4 ± 0.3	3.2
IL-2	18.9 ± 1.1 # Φ	20.2 ± 1.9 π θ	14.3 ± 1.1 # π	13.2 ± 0.9 Φ θ	3.2
IL-9	19.5 ± 1.0 # Φ	20.5 ± 1.6 π θ	16.4 ± 1.2 # π	15.2 ± 0.5 Φ θ	3.2
IL-1α	24.9 ± 2.3	26.5 ± 2.8	34.2 ± 4.4	27.5 ± 2.6	3.2
IL-1β	9.4 ± 0.3	9.5 ± 0.3	10.8 ± 0.6	9.8 ± 0.2	3.2
IFN-γ	24.3 ± 0.5	22.6 ± 0.6	25.0 ± 1.4	22.7 ± 0.8	3.2
IL-7	21.3 ± 0.7	18.9 ± 0.6	20.0 ± 0.8	20.2 ± 1.1	3.2
IL-12 (P40)	26.6 ± 1.0	23.3 ± 0.9	25.4 ± 1.0	23.3 ± 0.9	3.2

Values bearing identical designations (# or π or Φ or θ) within a row represent significant differences. Values in bold are significantly lower than those of the IL-33^{HET}/Tg+ group (n = 8–10). $p \leq 0.05$.

LOD, lowest limit of detection.

IL-33 deletion results in significant reduction in airway mucous cell density but without amelioration of muco-obstructive phenotype of Tg+ juveniles

To determine the effect of IL-33 deletion on mucus obstruction, we analyzed the airway luminal contents in AB-PAS–stained lung sections from WT and Tg+ mice on the IL-33^{HET} and IL-33^{KO} background. Although there was no sign of mucus plugging in IL-33^{HET}/WT as well as IL-33^{KO}/WT mice, the IL-33^{HET}/Tg+ mice had marked mucus obstruction (Fig. 4A). Contrary to our expectation, the degree of mucus obstruction was significantly increased in IL-33^{KO}/Tg+ mice versus IL-33^{HET}/Tg+ mice (Fig. 4A). This quantitative scoring was consistent with our visual observations, made while performing BALF collection, that IL-33^{KO}/Tg+ mice contained relatively larger mucus plugs (data not shown).

Increased mucous cell density (i.e., MCM) is a hallmark feature of Tg+ lung disease (15). To explore whether the sustained mucus obstruction in IL-33^{KO}/Tg+ mice results from increased mucous cell density, AB-PAS–stained lung sections were examined for intracellular mucopolysaccharide contents. AB-PAS–stained airway epithelial cells were sporadically present in the airways of IL-33^{HET}/WT but not in IL-33^{KO}/WT mice (Fig. 4B). Although the IL-33^{HET}/Tg+ airway epithelium had significantly higher numbers of AB-PAS–stained cells (Fig. 4B, 4C), the proportion of mucous cells was significantly reduced in IL-33^{KO}/Tg+ mice (Fig. 4B, 4D).

Absence of IL-33 has differential effect on the gene and protein expression of gel-forming mucins

To determine the effect of IL-33 deletion on gene expression of two major gel-forming mucins, *Muc5b* and *Muc5ac*, gene expression analyses was performed on total RNA from lungs. As reported previously (16), the *Muc5b* gene signatures were elevated in the IL-33^{HET}/Tg+ lungs (Fig. 5A). However, there was no significant difference in the *Muc5b* gene signatures in IL-33^{HET}/Tg+ versus IL-33^{KO}/Tg+ mice (Fig. 5A). As compared with WT counterparts, IL-33^{HET}/Tg+ and IL-33^{KO}/Tg+ mice had significantly elevated *Muc5ac* gene signatures (Fig. 5B). Although trending toward lower expression, the reduction in *Muc5ac* gene signature in IL-33^{KO}/Tg+ mice did not reach statistical significance (Fig. 5B). In addition, we performed in situ hybridization for the airway epithelium-specific expression patterns of *Muc5b* and *Muc5ac* transcripts. Both *Muc5b* and *Muc5ac* transcripts were almost equally abundant in the epithelial cells of large airways of IL-33^{HET}/Tg+ (Fig. 5C) as well as IL-33^{KO}/Tg+ (Fig. 5D) mice.

To explore the effect of IL-33 deletion on protein contents of both MUC5B and MUC5AC, their levels were determined in BALF. MUC5B levels were very low and comparable between IL-33^{HET}/WT and IL-33^{KO}/WT mice. As compared with their WT counterparts, the IL-33^{HET}/Tg+ and IL-33^{KO}/Tg+ mice had ∼9- and 12-fold higher MUC5B content, respectively. Although trending toward lower levels, the MUC5B contents in IL-33^{KO}/Tg+ mice were not significantly lower than IL-33^{HET}/Tg+ mice (Fig. 5E, left panel, Supplemental Fig. 2A). MUC5AC BALF contents were present at very low levels in the IL-33^{HET}/WT as well as IL-33^{KO}/WT mice but were found to be significantly elevated in IL-33^{HET}/Tg+ mice (Fig. 5F, right panel, Supplemental Fig. 2B). Importantly, as compared with IL-33^{HET}/Tg+ mice, the MUC5AC levels were significantly reduced to the baseline levels in IL-33^{KO}/Tg+ mice (Fig. 5F, right panel, Supplemental Fig. 2B).

Absence of IL-33 does not alter postnatal mortality, body weight, and prevalence of spontaneous bacterial infections in Tg+ offspring

The Tg+ mice on C57BL/6 background exhibit mortality within first 3 wk of postnatal life (13). To explore the contribution of IL-33 toward postnatal mortality in Tg+ mice, we observed pups from various breeding strategies (see *Materials and Methods* section) for any postnatal distress and mortality. Pups of all the four genotypes were born at expected Mendelian ratios, and as indicated by their body weights at the age of 3 wk, none of the offspring exhibited any signs of distress due to IL-33 deficiency (Supplemental Fig. 3A). Whereas ∼19% IL-33^{HET}/Tg+ pups did not survive beyond 3 wk of age, IL-33^{KO}/Tg+ pups exhibited a nonsignificant increase (∼23%) in mortality (Supplemental Fig. 3B). The status of IL-33 deficiency or Tg+ presence in parents undergoing reciprocal crossings had no obvious effect on the postnatal survival or body weights.

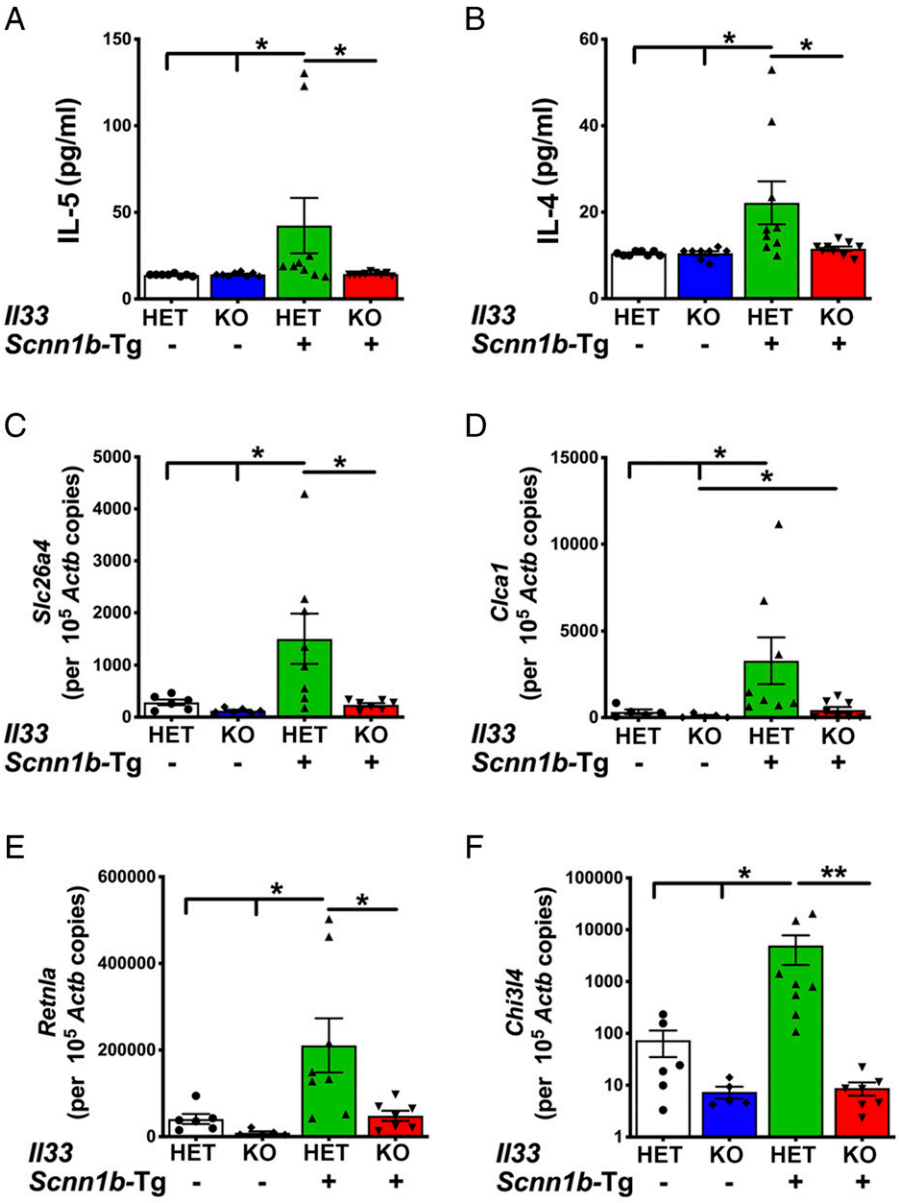

FIGURE 3. IL-33 deficiency suppresses molecular markers of *Th2* inflammation in juvenile Tg+ lungs. Cytokine levels (picograms per milliliter) of IL-5 (**A**) and IL-4 (**B**) in cell-free BALF from IL-33^{HET}/WT (white bar), IL-33^{KO}/WT (blue bar), IL-33^{HET}/Tg+ (green bar), IL-33^{KO}/Tg+ juveniles (red bar). Error bars represent SEM. Absolute quantification (mRNA copies per 1×10^5 copies of *Actb* mRNA) of mRNA for *Slc26a4* (**C**), *Clca1* (**D**), *Retnla* (**E**), and *Chi3l4* (**F**) in lung homogenate of IL-33^{HET}/WT (white bar), IL-33^{KO}/WT (blue bar), IL-33^{HET}/Tg+ (green bar), and IL-33^{KO}/Tg+ juveniles (red bar). Error bars represent SEM. $*p < 0.05$, $**p < 0.01$ using ANOVA followed by Tukey multiple comparison post hoc test.

To determine the effect of IL-33 deletion on bacterial clearance, we analyzed bacterial burden in aseptically collected BALF from neonates (PND 7) and juveniles (PND 21). In the absence of *Scnn1b* transgene, only 1 out of 10 IL-33^{HET}/WT (CFU ~3500) and 3 out of 16 IL-33^{KO}/WT (mean CFU ~125.9 ± 85.3) neonates had bacterial infection (Supplemental Fig. 3C). As compared with their WT counterparts, IL-33^{HET}/Tg+ and IL-33^{KO}/Tg+ neonates had a significantly higher degree of bacterial infection. Only 1 out of 12 IL-33^{HET}/Tg+ and 4 out of 14 IL-33^{KO}/Tg+ neonates had no signs of bacterial infection. Mean CFU counts in IL-33^{HET}/Tg+ (mean CFU ~$6.9 \times 10^4 \pm 3.7 \times 10^4$) were not significantly different from IL-33^{KO}/Tg+ neonates (mean CFU ~$6.1 \times 10^4 \pm 2.9 \times 10^4$) (Supplemental Fig. 3C).

Tg+ mice are known to clear airspace infection by the age of 3 wk (11). Only mild bacterial infection was detected in 7 out of 29 IL-33^{HET}/WT (mean CFU ~16.6 ± 8.5) and 7 out of 16 IL-33^{KO}/WT (mean CFU ~11.2 ± 3.8) juveniles (Supplemental Fig. 3D). In contrast, bacterial burden was significantly elevated in both IL-33^{HET}/Tg+ (mean CFU ~443.2 ± 231.4) and IL-33^{KO}/Tg+ (mean CFU ~59.4 ± 24.9) juveniles (Supplemental Fig. 3D). Although mean CFU counts were trending toward lower in IL-33^{KO}/Tg+ juveniles, the differences between IL-33^{KO}/Tg+ and IL-33^{HET}/Tg+ juveniles were statistically nonsignificant ($p = 0.12$) (Supplemental Fig. 3D).

IL-33 deletion modulates pulmonary pathology in Tg+ juveniles

The effects of IL-33 deletion on Tg+ pulmonary pathology, including airway inflammation, alveolar space enlargement, and lymphoid hyperplasia, were examined. Subepithelial/peribronchiolar airway inflammation with marked leukocytic infiltration is associated with Tg+ lung pathology (15). The airway inflammation was not evident in IL-33^{HET}/WT as well as IL-33^{KO}/WT groups. As previously reported (15), the peribronchiolar inflammation was present in IL-33^{HET}/Tg+ lungs (Fig. 6A). The inflammatory cellular infiltrates were an admixture of neutrophils, eosinophils, and lymphocytes (Fig. 6A). In contrast, the degree of neutrophilic and lymphocytic infiltration was significantly higher in IL-33^{KO}/Tg+ lungs (Fig. 6A). As reflected by the absence of eosinophils in IL-33^{KO}/Tg+ BALF, the peribronchiolar inflammation had negligible presence of eosinophils (Fig. 6A).

Alveolar space enlargement is a consistent feature of Tg+ lung disease (15). We performed semiquantitative (Fig. 6B; top) as well

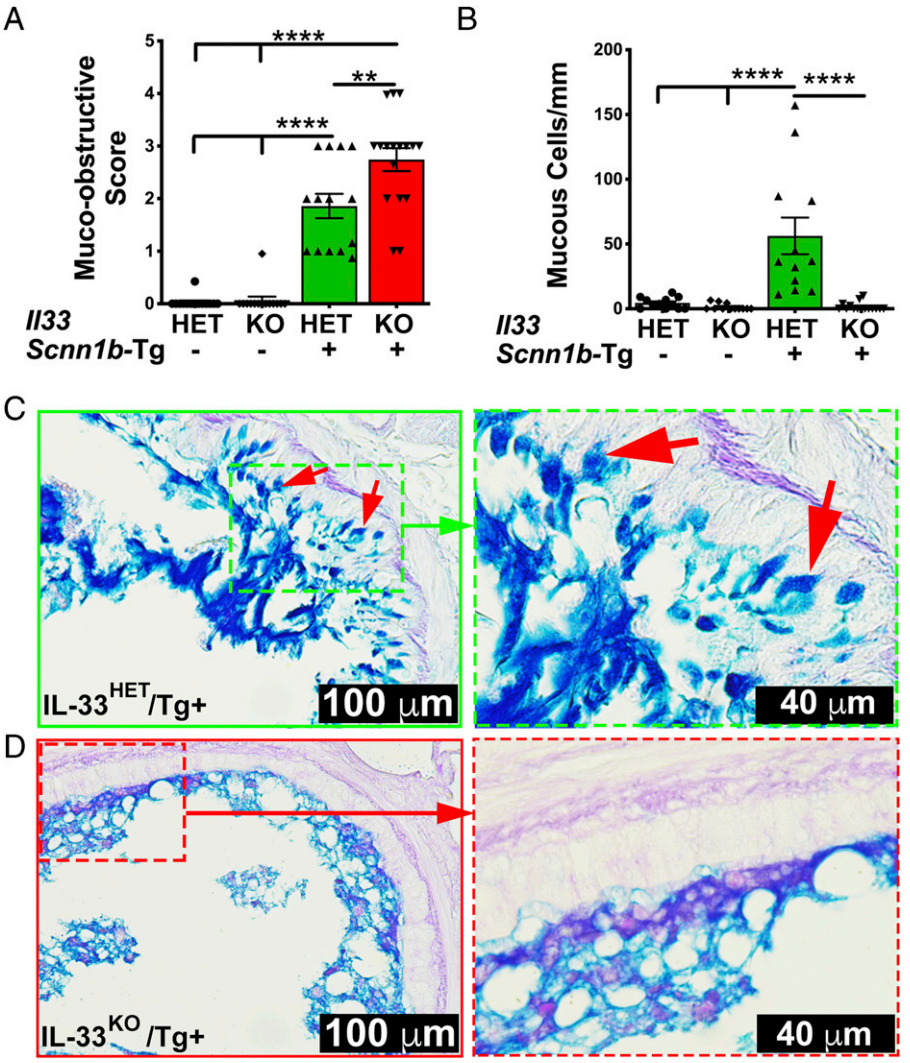

FIGURE 4. IL-33 deletion does not alleviate mucus obstruction despite significant suppression of mucous cell density in juvenile Tg+ airways. (**A**) Semiquantitative histological scoring for airway mucus obstruction in IL-33^{HET}/WT (white bar), IL-33^{KO}/WT (blue bar), IL-33^{HET}/Tg+ (green bar), and IL-33^{KO}/Tg+ juveniles (red bar). (**B**) Number of mucous cells per millimeter of basement membrane, IL-33^{HET}/WT (white bar), IL-33^{KO}/WT (blue bar), IL-33^{HET}/Tg+ (green bar), and IL-33^{KO}/Tg+ juveniles (red bar). (**C**) Representative photomicrograph of AB-PAS–stained left lung section from IL-33^{HET}/Tg+ (higher magnification of inset is shown as dotted green border). Intracellular AB-PAS staining of mucous cells is indicated by red arrows. (**D**) Representative photomicrograph of AB-PAS–stained left lung section from IL-33^{KO}/Tg+ (higher magnification of inset is shown as dotted red border). Error bars represent SEM. $^{**}p < 0.01$, $^{****}p < 0.0001$ using ANOVA followed by Tukey multiple comparison post hoc test.

as quantitative (MLI) analyses (Fig. 6B; bottom) on lung sections. Both IL-33^{HET}/WT and IL-33^{KO}/WT had comparable alveolar space sizes (Fig. 6B). As expected, alveolar space enlargement was a prominent feature of the IL-33^{HET}/Tg+ lungs but was widespread and significantly greater in IL-33^{KO}/Tg+ lungs (Fig. 6B).

Lymphoid hyperplasia (i.e., the appearance of lymphoid aggregates/nodules) is another pathological response present in Tg+ lungs (17, 18). Both IL-33^{HET}/WT and IL-33^{KO}/WT were completely devoid of lymphoid aggregates. Although 5 out of 12 IL-33^{HET}/Tg+ lungs had lymphoid aggregates, 9 out of 14 IL-33^{KO}/Tg+ mice had greater incidence of lymphoid aggregates with greater numbers per animal (Fig. 6C). However, this increase in prevalence of lymphoid aggregates in IL-33^{KO}/Tg+ mice was not statistically significant ($p = 0.15$).

Discussion

Our recent report demonstrated a positive correlation between increased levels of IL-33 in the muco-obstructive airspaces of Tg+ mice and robust MCM (9). Both responses were found suppressed in the secondhand smoke (SHS)–exposed Tg+ juveniles (9). Accordingly, we had proposed in our conceptual model that the ASL dehydration triggers IL-33 release from airway epithelial cells that, via downstream effector cells, orchestrate MCM in Tg+ airways (9). In addition, we conceptualized that the SHS exposure results in the suppression of IL-33 expression in airway epithelial cells that eventually leads to the suppression of MCM. This model led us to the next logical step of investigating the effect of germline deletion of IL-33 on the MCM and MCM-associated pathological features such as mucus obstruction, airway inflammation, and bacterial infection. In the current study, employing the IL-33^{KO}/Tg+ mouse, we have mechanistically tested our central hypothesis that IL-33 is essential for *Th2* inflammatory responses that contribute to the mucus obstruction in the airways of Tg+ mice.

The Tg+ lung disease follows a typical age-associated shift in inflammatory milieu in the airspaces that alters activation patterns of macrophages (16). Whereas M1 activation, a *Th1*-associated classical macrophage activation pattern, predominates in Tg+ at PND 3, the M2 activation, *Th2*-associated alternative macrophage activation, is robust at PND 10 and PND 42 (16). This trend likely suggests that the *Th1* response that coincides with the onset of spontaneous bacterial infection is switched to *Th2* responses during the second week of age. The levels of IL-33, a primary *Th2* response trigger, in Tg+ BALF confirm this correlation (i.e., absence of detectable IL-33 at PND 7 and significant presence of IL-33 at PND 21) (Fig. 1A). These data suggest that release of IL-33 into the airspaces, which occurs sometime between PND 7 and PND 21, likely mirrors *Th2* responses in Tg+ mice.

Upon allergen challenge, stressed epithelial cells release IL-33 that, along with IL-25 and TSLP, initiates *Th2*-predominated responses (19). The identity of trigger for IL-33 release in Tg+ airspaces remains unclear. Although ASL dehydration along with

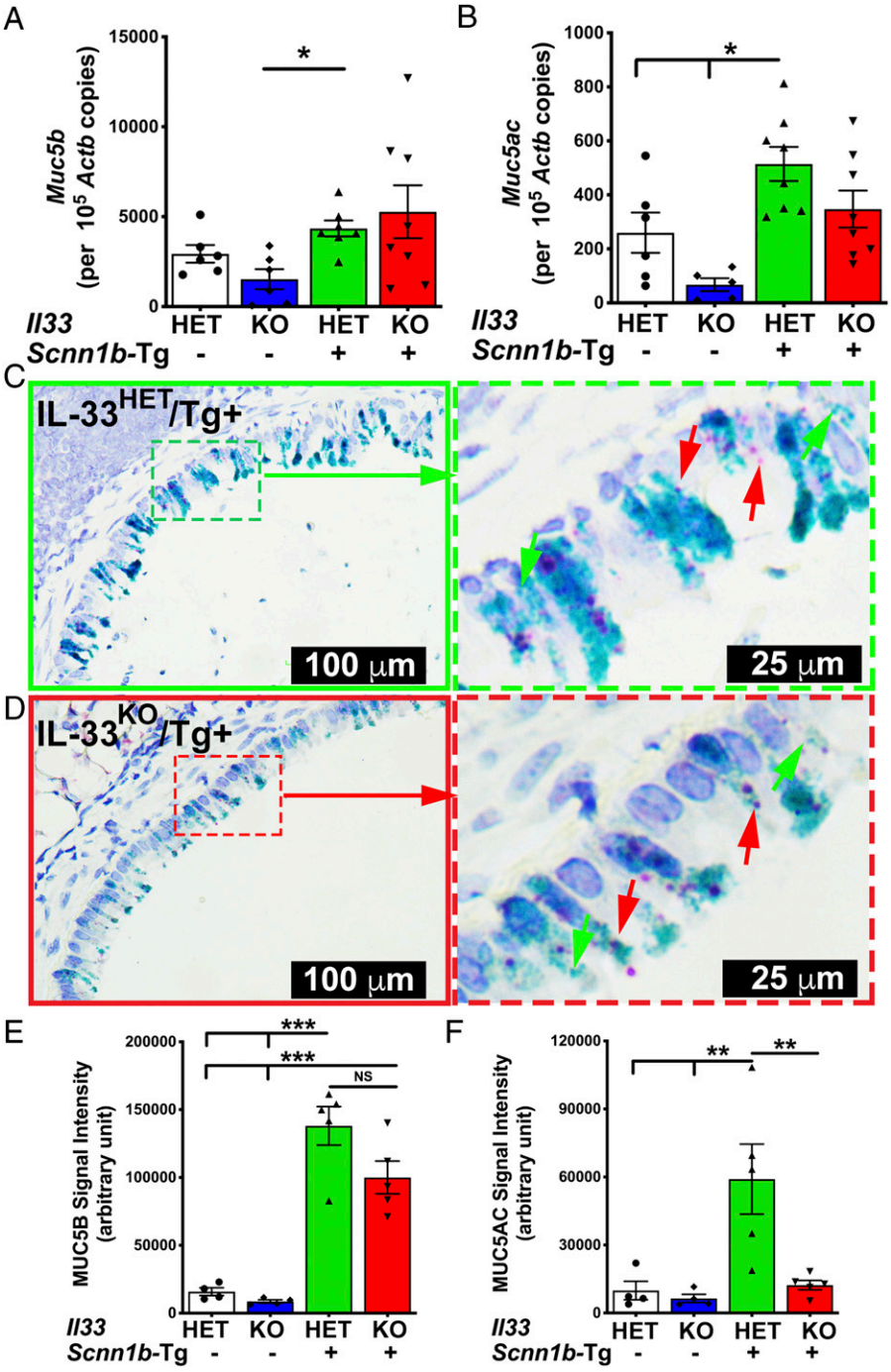

FIGURE 5. IL-33 deletion results in reduced MUC5AC but not MUC5B protein contents in juvenile Tg+ BALF. Absolute quantification (mRNA copies per 1×10^5 copies of *Actb* mRNA) of mRNA for *Muc5b* (**A**) and *Muc5ac* (**B**) in lung homogenate of IL-33^{HET}/WT (white bar), IL-33^{KO}/WT (blue bar), IL-33^{HET}/Tg+ (green bar), IL-33^{KO}/Tg+ (red bar) mice. Error bars represent SEM. $*p < 0.05$ using ANOVA followed by Tukey multiple comparison post hoc test. Representative photomicrograph from in situ mRNA hybridization (RNAScope) analyses of *Muc5b* (green stain) and *Muc5ac* (red stain) transcripts in lung sections from IL-33^{HET}/Tg+ (**C**) (higher magnification of inset is shown as dotted green border) and IL-33^{KO}/Tg+ (**D**) (higher magnification of inset is shown as dotted red border) mice. Western blot analyses for MUC5B (**E**) and MUC5AC (**F**) in the BALF from IL-33^{HET}/WT (white bar), IL-33^{KO}/WT (blue bar), IL-33^{HET}/Tg+ (green bar), IL-33^{KO}/Tg+ (red bar) mice. Error bars represent SEM. Images used for the quantification of agarose Western blot for MUC5B and MUC5AC are supplied as Supplemental Fig. 2. $**p < 0.01$, $***p < 0.001$ using ANOVA followed by Tukey multiple comparison post hoc test.

epithelial necrosis is evident well before PND 5 (15), the BALF from 7-d-old Tg+ pups did not show any evidence of IL-33 (Fig. 1A). It is likely that epithelial necrosis, a response seen during early neonatal stage (15), initiates IL-33 release from necrotic cells that achieve measurable concentration somewhere between PND 7 and PND 21. In contrast, because alveolar epithelial cells in Tg+ mice stained intensely for nuclear IL-33, the possibility exists that alveolar epithelial cells are the primary source of BALF IL-33 (Fig. 1B). Further studies using Tg+ mice with cell-specific (e.g., airway epithelium, alveolar epithelium, and immune cells) ablation of IL-33 are required to identify the cellular source of IL-33 in Tg+ mice.

In our recent report, mucus obstruction was significantly reduced in the SHS-exposed Tg+ mice (9). Strong association of this outcome with suppressed IL-33 expression and diminished MCM in the SHS-exposed Tg+ mice led to our hypothesis that the mucus obstruction would be significantly reduced in the absence of mucous cells in IL-33^{KO}/Tg+ lungs. Counterintuitively, our data reveal that the complete absence of mucous cells does not alleviate mucus obstruction from Tg+ airways (Fig. 4A–D). In other words, retention of ciliated cell density does not restore normal ciliary clearance function as well. It is therefore most likely that the accumulation of normally produced mucopolysaccharides in the dehydrated ASL layer of Tg+ mice, rather than increased mucous cell density, contributes to the pathologic mucus obstruction in Tg+ mice.

Our mRNA copy number analyses (RT-PCR–based gene expression and in situ RNA hybridization analyses) revealed that IL-33^{HET}/Tg+ as well as IL-33^{KO}/Tg+ mice had comparable copy numbers for *Muc5b* (Fig. 5A, 5C, 5D). Further, MUC5B protein contents were also not significantly different in the BALF

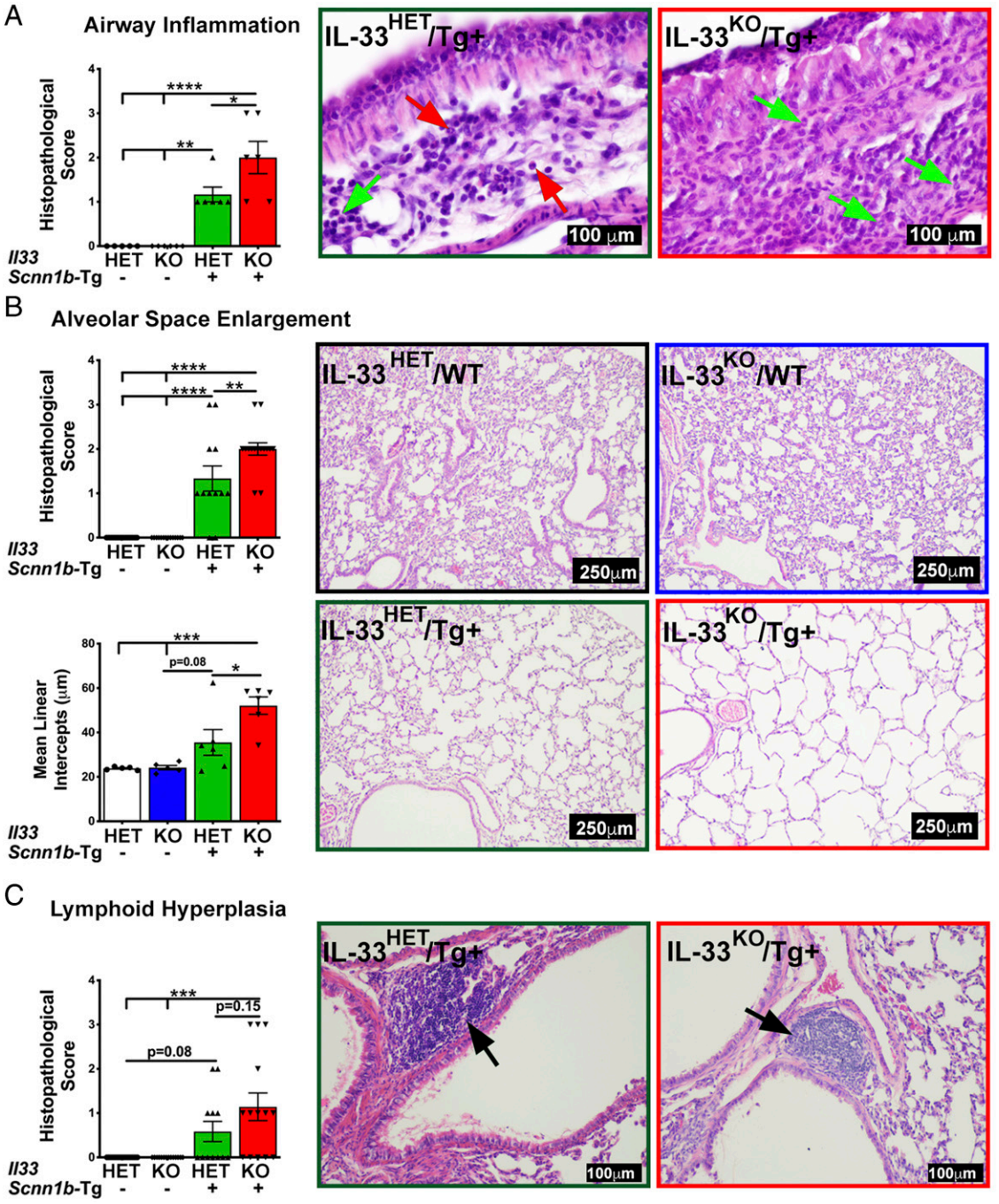

FIGURE 6. IL-33 deficiency modulates pulmonary pathology in Tg+ juveniles. (**A**) Semiquantitative histological scoring for airway inflammation in IL-33^{HET}/WT (white bar), IL-33^{KO}/WT (blue bar), IL-33^{HET}/Tg+ (green bar), and IL-33^{KO}/Tg+ juveniles (red bar). Representative photomicrographs from H&E-stained left lung lobe sections showing peribronchiolar inflammation in IL-33^{HET}/Tg+ (left panel) and IL-33^{KO}/Tg+ juveniles (right panel). Green and red arrows point to neutrophils and eosinophils, respectively. (**B**) Semiquantitative histological scoring (top bar graph) for alveolar space enlargement in IL-33^{HET}/WT (white bar), IL-33^{KO}/WT (blue bar), IL-33^{HET}/Tg+ (green bar), and IL-33^{KO}/Tg+ juveniles (red bar). Quantitative histological scoring (bottom bar graph) for MLI in IL-33^{HET}/WT (white bar), IL-33^{KO}/WT (blue bar), IL-33^{HET}/Tg+ (green bar), and IL-33^{KO}/Tg+ juveniles (red bar). Representative photomicrographs from H&E-stained left lung lobe sections from IL-33^{HET}/WT (black border), IL-33^{KO}/WT (blue border), IL-33^{HET}/Tg+ (green border) and IL-33^{KO}/Tg+ juveniles (red border). (**C**) Semiquantitative histological scoring for lymphoid hyperplasia in IL-33^{HET}/WT (white bar), IL-33^{KO}/WT (blue bar), IL-33^{HET}/Tg+ (green bar), IL-33^{KO}/Tg+ juveniles (red bar). Representative photomicrographs from H&E-stained left lung lobe sections showing lymphoid hyperplasia (black arrow) in IL-33^{HET}/Tg+ (left panel) and IL-33^{KO}/Tg+ juveniles (right panel). Error bars represent SEM. $^{*}p < 0.05$, $^{**}p < 0.01$, $^{***}p < 0.001$, $^{****}p < 0.000$ using ANOVA followed by Tukey multiple comparison post hoc test.

from IL-33^{HET}/Tg+ as well as IL-33^{KO}/Tg+ mice (Fig. 5E). In contrast, although the *Muc5ac* copy number was trending lower in IL-33^{KO}/Tg+ mice versus IL-33^{HET}/Tg+ mice (Fig. 5B), the MUC5AC protein contents were significantly lower in IL-33^{KO}/Tg+ mice versus IL-33^{HET}/Tg+ mice (Fig. 5F). The positive correlations between increased MUC5B, not MUC5AC, protein contents and the mucus obstruction have been recently reported (20). In this study, the complete loss of MUC5B (*Muc5b*$^{-/-}$/Tg+) resulted in significant reduction in the degree of mucus obstruction in Tg+ mice (20). However, the loss of MUC5AC (*Muc5ac*$^{-/-}$/Tg+) did not significantly

reduce the mucus obstruction in Tg+ mice (20). Along the same lines, although the IL-33^{KO}/Tg+ mice still had high MUC5B contents (Fig. 5E), the mucus obstruction was not alleviated despite significant reduction in MUC5AC protein contents (Fig. 5F). These data suggest that IL-33 does not regulate the transcription or translation of *Muc5b* mucin. It seems plausible that IL-33–independent pathways, including the recently implicated IL-1R–mediated pathway (21, 22), may regulate the expression of *Muc5b* in Tg+ mice.

IL-33 has been shown to increase neutrophil recruitment in response to bacterial infections (23, 24). In this study, we report that neutrophil counts and the levels of key neutrophil chemoattractants, such as KC, G-CSF, and MIP2, remain comparable between IL-33^{KO}/Tg+ and IL-33^{HET}/Tg+ BALF. These data suggest that IL-33–independent mechanisms are self-sufficient in neutrophil recruitment in response to spontaneous bacterial infections in Tg+ mice.

It has been shown that ILC2-derived IL-5 and IL-13 are essential for eosinophil recruitment, the deletion of IL-33R (ST2), however, does not completely inhibit eosinophil recruitment (25). In a recent report, Verma et al. (26) reported the existence of IL-13–expressing ILC2 in mice lacking ST2. These findings suggest the possible existence of IL-33–independent mechanisms for eosinophil recruitment whereby ILC2-derived IL-13 may induce eosinophil recruitment. However, eosinophil recruitment into Tg+ airways was abolished in the absence of IL-33 (i.e., scarce eosinophils were found only in 3 out of 14 IL-33^{KO}/Tg+ mice). These data suggest that the eosinophil recruitment to the Tg+ airways occurs via IL-33–responsive ILC2s.

The ASL dehydration in Tg+ is strongly associated with alveolar space enlargement (15). The IL-33^{KO}/Tg+ mice had significantly greater alveolar space enlargement, suggesting a protective role for IL-33 in this outcome. Two distinct cell-specific proteases, macrophage-specific matrix metalloproteinase 12 (MMP12) and neutrophil-specific neutrophil elastase (NE), have been implicated in the alveolar space enlargement response (27, 28). However, both neutrophil and macrophage counts in IL-33^{HET}/Tg+ and IL-33^{KO}/Tg+ mice were comparable. Because alveolar epithelial cells in IL-33^{HET}/Tg+ have upregulated expression of IL-33, it is possible that the loss of IL-33 in these cells make them susceptible to the alveolar space enlargement. Further studies are required to elucidate the mechanism by which IL-33 provides protection against excessive alveolar space enlargement.

In conclusion, this study revealed various findings on the involvement of IL-33 in the manifestation of muco-obstructive lung disease in Tg+ mice. First, IL-33 is essential for the recruitment of eosinophils in the airspaces of Tg+ mice. Second, the deletion of IL-33 results in the suppression of molecular markers of *Th2* inflammation in the Tg+ mice. Third, IL-33 is not essential for the transcription of *Muc5b* and *Muc5ac* genes; the translation of MUC5AC, however, is suppressed in the absence of IL-33. Fourth, although IL-33 deletion results in a significant reduction in mucous cell density, the mucus obstruction remains persistent in the Tg+ mice. Consequently, the postnatal mortality and bacterial infection remained persistent in the Tg+ mice. Finally, IL-33 provides protection against exaggerated airway inflammation and alveolar space enlargement. These findings indicate that deletion of IL-33 suppresses *Th2* responses but fails to correct MUC5B hyperconcentration and associated mucus obstruction in Tg+ airways. It remains unclear whether the MUC5B hyperconcentration and mucus obstruction are caused solely by the ASL dehydration or via IL-33–independent pathways.

Acknowledgments

We thank Thaya Stoufflet for assistance with multiplex cytokine assays and Sherry Ring for histological tissue processing.

Disclosures

The authors have no financial conflicts of interest.

References

1. Knowles, M. R., and R. C. Boucher. 2002. Mucus clearance as a primary innate defense mechanism for mammalian airways. *J. Clin. Invest.* 109: 571–577.
2. Boucher, R. C. 2007. Evidence for airway surface dehydration as the initiating event in CF airway disease. *J. Intern. Med.* 261: 5–16.
3. Boucher, R. C. 2007. Airway surface dehydration in cystic fibrosis: pathogenesis and therapy. *Annu. Rev. Med.* 58: 157–170.
4. Tarran, R. 2004. Regulation of airway surface liquid volume and mucus transport by active ion transport. *Proc. Am. Thorac. Soc.* 1: 42–46.
5. Mall, M., B. R. Grubb, J. R. Harkema, W. K. O'Neal, and R. C. Boucher. 2004. Increased airway epithelial Na+ absorption produces cystic fibrosis-like lung disease in mice. *Nat. Med.* 10: 487–493.
6. Dabbagh, K., K. Takeyama, H. M. Lee, I. F. Ueki, J. A. Lausier, and J. A. Nadel. 1999. IL-4 induces mucin gene expression and goblet cell metaplasia in vitro and in vivo. *J. Immunol.* 162: 6233–6237.
7. Zhu, Z., R. J. Homer, Z. Wang, Q. Chen, G. P. Geba, J. Wang, Y. Zhang, and J. A. Elias. 1999. Pulmonary expression of interleukin-13 causes inflammation, mucus hypersecretion, subepithelial fibrosis, physiologic abnormalities, and eotaxin production. *J. Clin. Invest.* 103: 779–788.
8. Schmitz, J., A. Owyang, E. Oldham, Y. Song, E. Murphy, T. K. McClanahan, G. Zurawski, M. Moshrefi, J. Qin, X. Li, et al. 2005. IL-33, an interleukin-1-like cytokine that signals via the IL-1 receptor-related protein ST2 and induces T helper type 2-associated cytokines. *Immunity* 23: 479–490.
9. Lewis, B. W., R. Sultana, R. Sharma, A. Noël, I. Langohr, S. Patial, A. L. Penn, and Y. Saini. 2017. Early postnatal secondhand smoke exposure disrupts bacterial clearance and abolishes immune responses in muco-obstructive lung disease. *J. Immunol.* 199: 1170–1183.
10. Oboki, K., T. Ohno, N. Kajiwara, K. Arae, H. Morita, A. Ishii, A. Nambu, T. Abe, H. Kiyonari, K. Matsumoto, et al. 2010. IL-33 is a crucial amplifier of innate rather than acquired immunity. *Proc. Natl. Acad. Sci. USA* 107: 18581–18586.
11. Livraghi-Butrico, A., E. J. Kelly, E. R. Klem, H. Dang, M. C. Wolfgang, R. C. Boucher, S. H. Randell, and W. K. O'Neal. 2012. Mucus clearance, MyD88-dependent and MyD88-independent immunity modulate lung susceptibility to spontaneous bacterial infection and inflammation. *Mucosal Immunol.* 5: 397–408.
12. Saini, Y., K. J. Wilkinson, K. A. Terrell, K. A. Burns, A. Livraghi-Butrico, C. M. Doerschuk, W. K. O'Neal, and R. C. Boucher. 2016. Neonatal pulmonary macrophage depletion coupled to defective mucus clearance increases susceptibility to pneumonia and alters pulmonary immune responses. *Am. J. Respir. Cell Mol. Biol.* 54: 210–221.
13. Livraghi, A., B. R. Grubb, E. J. Hudson, K. J. Wilkinson, J. K. Sheehan, M. A. Mall, W. K. O'Neal, R. C. Boucher, and S. H. Randell. 2009. Airway and lung pathology due to mucosal surface dehydration in beta-epithelial Na+ channel-overexpressing mice: role of TNF-alpha and IL-4Ralpha signaling, influence of neonatal development, and limited efficacy of glucocorticoid treatment. *J. Immunol.* 182: 4357–4367.
14. Ramsey, K. A., Z. L. Rushton, and C. Ehre. 2016. Mucin agarose gel electrophoresis: western blotting for high-molecular-weight glycoproteins. *J. Vis. Exp.* 112: e54153.
15. Mall, M. A., J. R. Harkema, J. B. Trojanek, D. Treis, A. Livraghi, S. Schubert, Z. Zhou, S. M. Kreda, S. L. Tilley, E. J. Hudson, et al. 2008. Development of chronic bronchitis and emphysema in beta-epithelial Na+ channel-overexpressing mice. *Am. J. Respir. Crit. Care Med.* 177: 730–742.
16. Saini, Y., H. Dang, A. Livraghi-Butrico, E. J. Kelly, L. C. Jones, W. K. O'Neal, and R. C. Boucher. 2014. Gene expression in whole lung and pulmonary macrophages reflects the dynamic pathology associated with airway surface dehydration. *BMC Genomics* 15: 726.
17. Saini, Y., B. W. Lewis, D. Yu, H. Dang, A. Livraghi-Butrico, F. Del Piero, W. K. O'Neal, and R. C. Boucher. 2018. Effect of LysM+ macrophage depletion on lung pathology in mice with chronic bronchitis. *Physiol. Rep.* 6: e13677.
18. Livraghi-Butrico, A., B. R. Grubb, E. J. Kelly, K. J. Wilkinson, H. Yang, M. Geiser, S. H. Randell, R. C. Boucher, and W. K. O'Neal. 2012. Genetically determined heterogeneity of lung disease in a mouse model of airway mucus obstruction. *Physiol. Genomics* 44: 470–484.
19. Hammad, H., M. Chieppa, F. Perros, M. A. Willart, R. N. Germain, and B. N. Lambrecht. 2009. House dust mite allergen induces asthma via toll-like receptor 4 triggering of airway structural cells. *Nat. Med.* 15: 410–416.
20. Livraghi-Butrico, A., B. R. Grubb, K. J. Wilkinson, A. S. Volmer, K. A. Burns, C. M. Evans, W. K. O'Neal, and R. C. Boucher. 2017. Contribution of mucus concentration and secreted mucins Muc5ac and Muc5b to the pathogenesis of muco-obstructive lung disease. *Mucosal Immunol.* 10: 395–407.
21. Fritzsching, B., Z. Zhou-Suckow, J. B. Trojanek, S. C. Schubert, J. Schatterny, S. Hirtz, R. Agrawal, T. Muley, N. Kahn, C. Sticht, et al. 2015. Hypoxic epithelial necrosis triggers neutrophilic inflammation via IL-1 receptor signaling in cystic fibrosis lung disease. *Am. J. Respir. Crit. Care Med.* 191: 902–913.
22. Chen, G., L. Sun, T. Kato, K. Okuda, M. B. Martino, A. Abzhanova, J. M. Lin, R. C. Gilmore, B. D. Batson, Y. K. O'Neal, et al. 2019. IL-1β dominates the promucin secretory cytokine profile in cystic fibrosis. *J. Clin. Invest.* 129: 4433–4450.
23. Robinson, K. M., K. Ramanan, M. E. Clay, K. J. McHugh, H. E. Rich, and J. F. Alcorn. 2018. Novel protective mechanism for interleukin-33 at the mucosal

barrier during influenza-associated bacterial superinfection. *Mucosal Immunol.* 11: 199–208.

24. Lan, F., B. Yuan, T. Liu, X. Luo, P. Huang, Y. Liu, L. Dai, and H. Yin. 2016. Interleukin-33 facilitates neutrophil recruitment and bacterial clearance in *S. aureus*-caused peritonitis. *Mol. Immunol.* 72: 74–80.
25. Iijima, K., T. Kobayashi, K. Hara, G. M. Kephart, S. F. Ziegler, A. N. McKenzie, and H. Kita. 2014. IL-33 and thymic stromal lymphopoietin mediate immune pathology in response to chronic airborne allergen exposure. *J. Immunol.* 193: 1549–1559.
26. Verma, M., S. Liu, L. Michalec, A. Sripada, M. M. Gorska, and R. Alam. 2018. Experimental asthma persists in IL-33 receptor knockout mice because of the emergence of thymic stromal lymphopoietin-driven IL-9^+ and IL-13^+ type 2 innate lymphoid cell subpopulations. *J. Allergy Clin. Immunol.* 142: 793–803.e8.
27. Gehrig, S., J. Duerr, M. Weitnauer, C. J. Wagner, S. Y. Graeber, J. Schatterny, S. Hirtz, A. Belaaouaj, A. H. Dalpke, C. Schultz, and M. A. Mall. 2014. Lack of neutrophil elastase reduces inflammation, mucus hypersecretion, and emphysema, but not mucus obstruction, in mice with cystic fibrosis-like lung disease. *Am. J. Respir. Crit. Care Med.* 189: 1082–1092.
28. Trojanek, J. B., A. Cobos-Correa, S. Diemer, M. Kormann, S. C. Schubert, Z. Zhou-Suckow, R. Agrawal, J. Duerr, C. J. Wagner, J. Schatterny, et al. 2014. Airway mucus obstruction triggers macrophage activation and matrix metalloproteinase 12-dependent emphysema. *Am. J. Respir. Cell Mol. Biol.* 51: 709–720.